# Hydraulic Interpretation of Direct Velocity Measurements in the Bab al Mandab*

L. J. PRATT

*Woods Hole Oceanographic Institution, Woods Hole, Massachusetts*

WILLIAM JOHNS

*Rosenstiel School of Marine and Atmospheric Sciences, University of Miami, Miami, Florida*

STEPHEN P. MURRAY

*Coastal Studies Institute, Louisiana State University, Baton Rouge, Louisiana*

KATSUROU KATSUMATA

*Department of Earth and Planetary Physics, University of Tokyo, Tokyo, Japan*

(Manuscript received 5 February 1997, in final form 14 October 1998)

ABSTRACT

Acoustic Doppler Current Profiler velocity measurements in the Bab al Mandab during the period June 1995–March 1996 are used to assess the hydraulic character of the exchange flow. The strait is 150 km long and contains two distinct geometrical choke points: the Hanish sill and Perim narrows. The authors use a three-layer approximation of the monthly mean velocity and density structure at the sill and narrows to calculate the phase speeds of the first and second internal, long gravity waves. The first (second) mode is generally characterized by in-phase (out-of-phase) motions of the two interfaces. The calculations take cross-strait topographic variations into consideration by using a piecewise linear representation of the actual bottom. The resulting phase speeds are used to determine whether the flow is subcritical, supercritical, or critical with respect to the first and second modes. Subcritical (supercritical) means that the two wave pairs corresponding to a given mode propagate in opposite (the same) directions, whereas ''critical'' means that one or both members of a pair has zero phase speed. Critical or supercritical conditions are indications of hydraulic control and imply that signal propagation through the strait associated with a particular mode can occur in only one direction, or perhaps not at all.

During the summer months, the velocity profiles indicate a ''three-layer'' structure, with surface water outflowing from the Red Sea, intermediate water inflowing from the Gulf of Aden, and Red Sea Water outflowing at the bottom. During this time period, the flow is found to be subcritical with respect to both internal modes, although tides and mesoscale disturbances are potentially strong enough to temporarily create critical or supercritical conditions, particularly with respect to the second internal mode at the narrows. During the winter and transitional months the velocity has a two-layer character with inflowing surface water and outflowing Red Sea Water. However, the outflowing Red Sea Water can further be partitioned into an intermediate layer originating from the Red Sea thermocline and a deeper, homogeneous layer originating from below the thermocline. A subtle three-layer character therefore exists and the three-layer model is configured accordingly. Surprisingly, the monthly mean narrows flow during this time period is found to be substantially subcritical with respect to the first baroclinic mode. At the Hanish sill the flow is marginally to moderately subcritical with respect to the first mode, suggesting the possibility of proximity to a section of critical control. It is possible that friction may be strong enough to shift the control section to the south of the sill. With respect to the second mode, the flow at both the Hanish sill and Perim narrows are found to be very close to the critical speed with respect to the second internal mode, suggesting hydraulic control. The wave whose propagation is arrested is one attempting to move from the Gulf of Aden into the Red Sea. The vertical structure of this wave suggests a role in determining how much Upper Red Sea Deep Water is able to pass through the Bab al Mandab and into the Gulf of Aden. The strength of tides and mesoscale disturbances in the strait suggest that this upstream influence may be intermittent.

Estimation of internal Rossby radii of deformation for the first and second internal modes indicates that rotation (which is neglected in our wave speed calculations) is only moderately weak. Nevertheless, the errors in calculated propagation speeds due to the neglect of rotation are estimated to be quite small.

* Woods Hole Oceanographic Institute Contribution Number 9649.

*Corresponding author address:* Dr. Larry J. Pratt, Woods Hole Oceanographic Institution, MS 21, 360 Woods Hole Rd., Woods Hole, MA 02543-1541.
E-mail: lpratt@whoi.edu

## 1. Introduction

The Bab al Mandab (BAM) is a strait 150 km long that connects the Red Sea to the Indian Ocean's Gulf of Aden (Fig. 1). The Red Sea is otherwise closed except for the Suez Canal, and the throughflow permitted in the latter is negligible. It has been well documented (e.g., Siedler 1968; Patzert 1974; Maillard and Soliman 1986; Smeed 1997) that winter conditions in the BAM consist of surface inflow into the Red Sea and deep outflow into the Gulf of Aden. The outflow originates from 50 to 200 m in the Red Sea with a smaller portion originating from greater depths. It forms an overflowing plume that descends from the 163-m-deep Hanish sill to 400–600 m in the Gulf of Aden (Fedorov and Mechanov 1988; Bower and Price 1999). This exchange flow is driven by 2 m $yr^{-1}$ evaporation and by cooling over the Red Sea and is probably reinforced by the monsoonal winds that blow more or less in the direction of the surface inflow during winter. In summer, the wind direction over the BAM reverses and a shallow (<20 m) surface outflow into the Gulf of Aden forms. The Red Sea inflow during this season lies beneath the surface layer and is composed primarily of Gulf of Aden Intermediate Water (Patzert 1974; Smeed 1997). Underneath this inflow is a weakened Red Sea outflow. Figure 1 shows that the sill, named after the nearby Hanish Islands, lies well north of the narrowest section, named after Perim Island. In the following, the terms ''sill'' or ''Hanish sill'' will refer to the cross section coincident with position B2 in Fig. 1, while the Perim narrows (or just ''narrows'') refers to the section at A2. The narrows generally contains the largest velocities. Also, the terms ''outflow'' and ''inflow'' will be used to indicate flow from and into the Red Sea, respectively.

Recent observations (Murray and Johns 1997) of the currents and stratification in the BAM apparently yield a paradox. On one hand, the strong upstream/downstream asymmetry of the flow strongly suggests that hydraulic control exists at the strait, perhaps at the sill or narrows. In particular, the overflow has the character of fluid spilling over a dam and qualitatively resembles the Mediterranean overflow and others that are known to be hydraulically controlled (Farmer and Armi 1988; Armi and Farmer 1988). On the other hand, rough estimates of the internal Froude number (Murray and Johns 1997) during the period of strongest exchange and based on direct velocity measurements at the narrows suggest that the flow is substantially subcritical with respect to the first internal long gravity mode. That is, ''two-layer'' internal gravity waves can propagate in

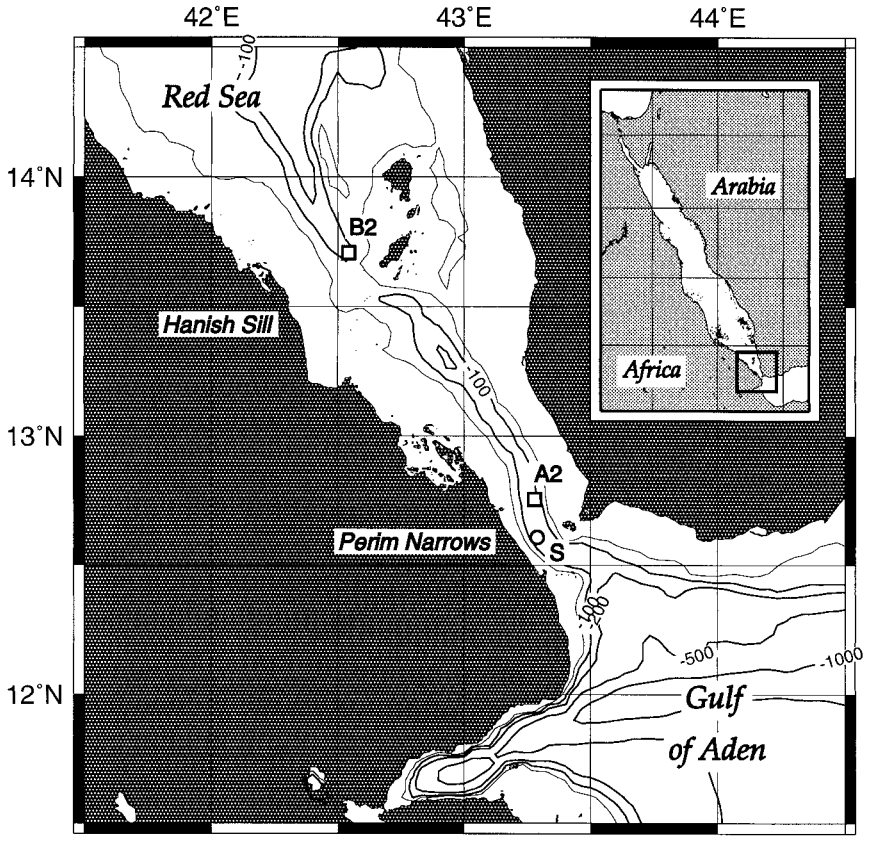


FIG. 1. Map of Bab al Mandab showing Hanish sill and Perim narrows sections. The site of Siedler's (1968) measurements are denoted by an ''S.''

both directions (toward the Red Sea and toward the Gulf of Aden), a feature that indicates a lack of hydraulic control at the narrows.

The number of possible configurations that hydraulically controlled three-layer flow can take is large (Smeed 1999, manuscript submitted to *J. Phys. Oceanogr.*), and this makes it difficult to anticipate what a hydraulically controlled summer flow in the BAM might look like. In the winter the situation is apparently simpler and elementary two-layer hydraulic theory (e.g., Farmer and Armi 1986) suggests one of the following regimes. First, the winter flow might be *maximally controlled,* meaning that supercritical motion would exist at either end of the strait. These supercritical flows would be joined to the slower flows in the Gulf of Aden and Red Sea by internal hydraulic jumps. Such a regime would prevent internal waves from propagating through the BAM in either direction. The presence of a strong seasonal cycle, in which the summer outflow is attenuated, suggest that long internal waves can propagate out of the strait from the Red Sea, arguing against maximal exchange. The other possible controlled state would be *submaximal,* a regime with supercritical flow at the southern end of the strait. Supposing that the sill and narrows represent the most likely locations of critical control, there are a number of configurations that might arise. A control section might exist at the sill, with supercritical flow to the south extending through the narrows and into the Gulf of Aden. This regime seems at odds with the observation of descending outflow into the Gulf of Aden. Or the flow could be subcritical to the north of the narrows (including the sill) and supercritical to the south. It is also possible for the flow to be critical at the sill, supercritical immediately downstream, and critical again at the narrows. In this case a hydraulic jump would exist between the sill and narrows. Further complicating the picture is that the winter flow appears to have a subtle three-layer character, as explained below.

Hydraulic conditions within the BAM during different seasons are important in many respects. Perhaps the most basic scientific issue concerns the extent to which the Red Sea stratification and thermohaline circulation are determined by local atmospheric forcing. The degree to which the Red Sea is self-contained and self-determined, and not just a gulf of the Indian Ocean, depends to a great extent on the ability of internal waves to propagate into the Red Sea through the BAM. Information concerning the propagation of waves is also important in the formulation of numerical models of the Red Sea in which open boundary conditions must be imposed at or near the BAM. For example, standard radiation conditions permitting wave propagation out of, but not into, the numerical domain may imply the existence of hydraulic control. Similar issues arise in the application of simple analytical models of the Red Sea thermohaline circulation (Phillips 1966; Maxworthy 1997), in which the investigator must decide whether or not to impose a critical control condition in the BAM. (Maxworthy did and Phillips did not.) Also, hydraulic control usually implies the existence of hydraulic jumps, whereby supercritical flow is returned to a subcritical state. Such jumps can lead to overturning and mixing within and between different layers and may be important, for example, in the mixing of the descending Gulf of Aden plume. Finally, the presence or lack of hydraulic controls within the strait is a contributing factor in the understanding of the stratification, velocity and overall local character of the exchange flow as suggested above.

In this paper we examine the question of flow criticality more thoroughly using monthly mean velocities obtained by Murray and Johns (1997) from Acoustic Doppler Current Profilers (ADCPs) moored at the Hanish sill and Perim narrows over the period June 1995 through March 1996. From these measurements and from hydrographic data obtained during the same period, we construct a local three-layer representation of the internal structure of each monthly mean flow using approximations to the cross-strait sill and narrows bottom topography. During summer months the three layers correspond to the outflowing surface and bottom layers, and inflowing intermediate layer described above. In the winter, the velocity structure has a two-layer character but the density has a three-layer structure (Siedler 1968), and we construct our three-layer model accordingly. In both cases, any net (barotropic) transport into or out of the Red Sea is removed. The propagation speeds of the first, internal, long gravity modes of the model flow are calculated, and it is found that the flow is subcritical with respect to these two-layer modes during each month. During the winter, the speed of one of these modes is reduced at the sill, indicating a possible two-layer internal hydraulic control in the vicinity. Such a control would prevent propagation of first internal gravity modes from the Gulf of Aden into the Red Sea. The model also permits calculation of the second (''mode 2'') internal long gravity wave speeds and the flows at the sill and narrows turns out to be subcritical with respect to these during the summer. During the winter, and perhaps the transition months, the flow at both the sill and narrows is close to the critical speed for mode 2. This result suggests the presence of a mode-2 hydraulic control associated the blockage of signals propagating from the Gulf of Aden into the Red Sea. The vertical structure of the wave that is arrested suggests that the control is instrumental in determining the percentage of Upper Red Sea Deep Water that composes the outflow.

The paper is organized as follows: Our three-layer model is described in section 2 and the wave speed calculations from it are presented in section 3 (for the Hanish sill) and section 4 (for the Perim narrows). In section 5 we discuss the composition of the winter outflow in more detail and discuss the ramifications of hydraulic control with respect to mode 2 on this composition. Section 6 discusses the potential importance of rotation and time dependence, both of which are neglected in the preceding analysis, and section 7 summarizes our findings.

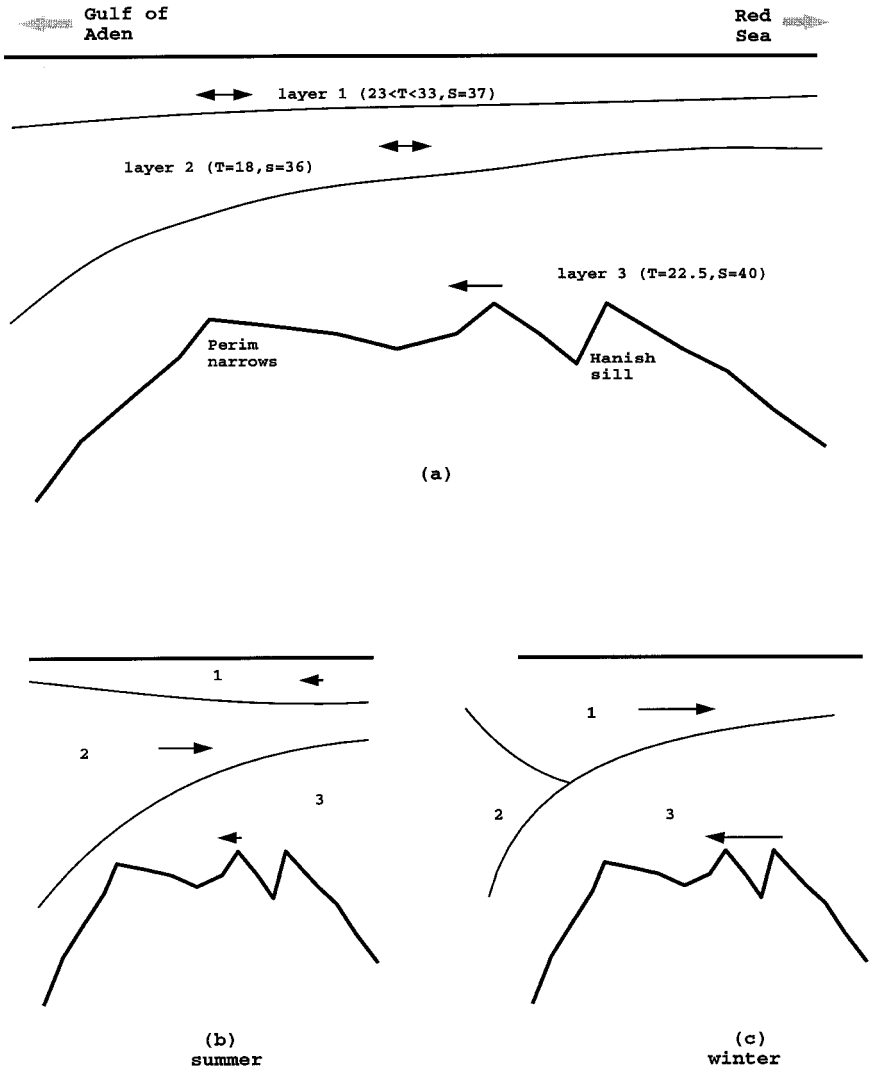


FIG. 2. Layer structure of Bab al Mandab exchange flow according to Smeed (1997).

## 2. The three-layer model

Based on historical XBT data, Smeed (1997) has approximated the stratification in the BAM by the summer and winter three-layer regimes shown in Fig. 2a. The surface layer has salinity ~37 psu and a temperature that varies seasonally over 23°–33°C. During the summer months, this layer is relatively thin (<20 m thickness) and warm (~32°C), and it flows toward the Gulf of Aden (Fig. 2b). During the winter months the layer is thicker (~80 m), cooler (~26°C) and it flows toward the Red Sea. The second layer is composed of cooler ($T \cong 18$°C) and slightly fresher ($S \cong 36$ psu) Gulf of Aden Intermediate Water (GAIW). In the summer, this layer flows into the Red Sea (Fig. 2b), forming an intrusion that has been detected as far as 800 km into that body (Smeed 1997). In the winter the intrusion retreats into the Gulf of Aden (or simply decays) and disappears from the BAM altogether, as suggested in Fig. 2c. As stated earlier the reversal in the direction of layers 1 and 2 are associated with the reversal of the monsoon winds in the southern Red Sea (Patzert 1974). The third and deepest layer is composed of Red Sea water originating from middepths (50–200 m) and, to some extent, greater depths. Layer 3 flows into the Gulf of Aden throughout the year, although the transport is attenuated during the summer.

Based partly on this picture of the stratification and partly on the observations of Murray and Johns (1997), we have constructed a three-layer model for calculating the propagation speeds of long, internal gravity waves at the sill and narrows. Each layer has uniform density and velocity. The model ignores lateral variations in layer velocities as well as the earth's rotation, and justification for the latter will be taken up in the final section. Two pairs of wave speeds are calculated, one for the first internal modes and the other for the second internal modes. Application of the model during the

months July, August, and September is straightforward as the velocity has the distinct three-layer structure shown in Fig. 2b. During the winter and transitional months (Oct–Mar) only layers 1 and 3 are present in the BAM as shown in Fig. 2c. However, the density distribution during this time period will show that layer 3 is actually composed of two sublayers so that the exchange flow has a three-layer structure apparent in density if not velocity. This feature, which was first recognized by Siedler[1] (1968), will be discussed more thoroughly in sections 3–5. In any case, we will continue to apply the three-layer model during this period, keeping in mind that the two-layer hydraulic character of the flow will be revealed by the mode-1 propagation speeds.

The bottom depth at the sill and narrows varies quite a bit, with deep central channels and shallow shelves, and use of a one-dimensional model in this situation would lead to obvious ambiguities in estimating layer depths. We have therefore derived general expressions for the propagation speeds over arbitrary cross-sectional topography. We will use these expressions in connection with shapes that approximate the actual geometry at the sill and narrows. Following the definition sketches of Fig. 3 consider a three-layer flow in the $x$ direction, contained in a channel whose bottom elevation varies with $y$. The layer densities, thicknesses, and velocities are denoted $\rho_n$, $d_n$, $u_n$ where ($n = 1, 2, 3$), and the departures of the interfaces from their equilibrium elevations are denoted $\eta_1$ and $\eta_2$. The hydrostatic, Boussinesq momentum equations governing the three layers are given by

$$\frac{\partial u_1}{\partial t} + \frac{\partial}{\partial x}\left(\frac{u_1^2}{2} + \frac{p_0}{\rho}\right) = 0$$

$$\frac{\partial u_2}{\partial t} + \frac{\partial}{\partial x}\left(\frac{u_2^2}{2} + \frac{p_0}{\rho} + g_1'\eta_1\right) = 0$$

$$\frac{\partial u_3}{\partial t} + \frac{\partial}{\partial x}\left(\frac{u_3^2}{2} + \frac{p_0}{\rho} + g_1'\eta_1 + g_2'\eta_2\right) = 0, \quad (2.1)$$

where

$$g_1' = g\frac{\rho_2 - \rho_1}{\rho} \quad \text{and} \quad g_2' = g\frac{\rho_3 - \rho_2}{\rho}.$$

In addition $\rho$ is the average density and $p_0$ is the pressure at the (rigid) upper surface.

Denoting the cross-sectional areas of each layer by $A_n$, the continuity equation for the $n$th layer is

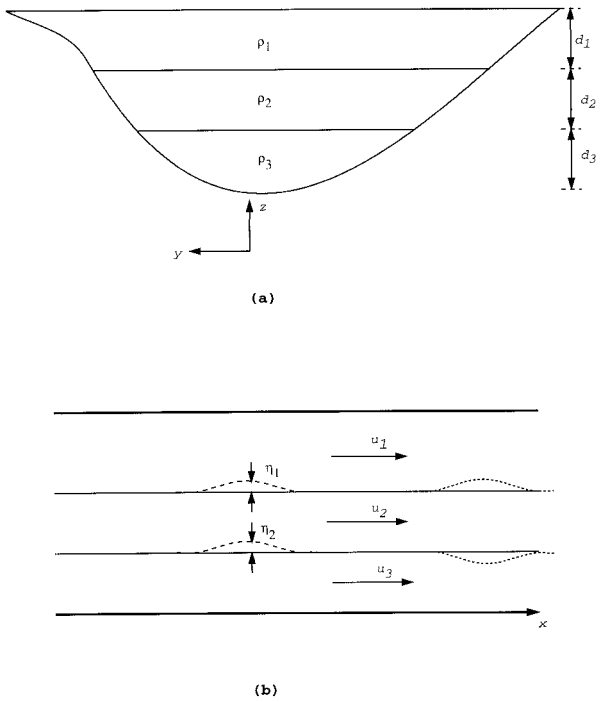


FIG. 3. Definition sketch showing (a) cross section and (b) longitudinal section for a three-layer model with continuously varying cross-sectional topography.

$$\frac{\partial A_n}{\partial t} = \frac{\partial (u_n A_n)}{\partial x}. \quad (2.2)$$

Following Baines (1995) treatment of the two-layer version of this problem, it is convenient to introduce the *shear* velocities

$$\nu_1 = u_1 - u_2 \quad \text{and} \quad \nu_2 = u_2 - u_3 \quad (2.3)$$

and to use these in place of the layer velocities through the substitutions

$$u_1 = \frac{Q + \nu_1 A_2 + (\nu_1 + \nu_2)A_3}{A}$$

$$u_2 = \frac{Q - \nu_1 A_1 + \nu_2 A_3}{A}$$

$$u_3 = \frac{Q - \nu_2 A_2 - (\nu_1 + \nu_2)A_1}{A}, \quad (2.4)$$

where

$$Q = u_1 A_1 + u_2 A_2 + u_3 A_3 \quad (2.5)$$

is the total (or ''barotropic'') volume transport and

$$A = A_1 + A_2 + A_3 \quad (2.6)$$

is the total cross-sectional area. Both $Q$ and $A$ are independent of $x$. At this stage no linearization has been made and the system contains the five unknowns ($\nu_1$, $\nu_2$, $\eta_1$, $\eta_2$, $p_0$). (Although the layer areas also appear to be variables, they depend only on the interface dis-

[1] In analyzing hydrographic data taken from near the narrows, Siedler (1968) was the first to recognize the three-layer structure of the winter flow and wrote ''The vertical distribution of temperature, salinity, and density is characterized by three layers: A homogeneous surface layer, a complicated intermediate layer with great variations in time, and an almost homogeneous bottom layer.'' (His narrows $\sigma_\theta$ profile is reproduced in our Fig. 11.)

placements.) The barotropic transport $Q$ is a parameter that must be predetermined for the case of a rigid lid and is negligibly small in our monthly mean BAM application. The barotropic pressure $p_0$ can be eliminated from consideration by subtracting any two of the momentum equations from each other. Two equations obtained this way and any two of (2.2) now comprise a 4 by 4 system for the unknowns ($\nu_1$, $\nu_2$, $\eta_1$, $\eta_2$).

We wish to calculate the propagation speeds of small disturbances to a steady background flow causing perturbations of the velocity and interface elevation $u_n'$ and $\eta_n$. We therefore replace $u_n$ by $u_n + u_n'$ and $d_n$ by ($d_1 - \eta_1$, $d_2 + \eta_1 - \eta_2$, and $d_3 + \eta_2$), where $u_n$ and $d_n$ now denote background velocity and thickness. These expressions are substituted into the 4 by 4 system suggested above and the resulting equations are linearized. In doing so the quadratic velocity terms $u_n \partial u_n/\partial x$ are replaced by $u_n \partial u_n'/\partial x$, and the layer areas are approximated as

$$A_1(d_1 - \eta_1(x, t)) \cong A_1(d_1) - \frac{dA_1}{d(d_1)}\eta_1(x, t),$$

for example. Carrying out similar expansions for $A_2$ and $A_3$ results, after some tedious algebra, in the system

$$\frac{\partial \nu_i}{\partial t} + a_{ij}\frac{\partial \nu_j}{\partial x} = 0, \tag{2.7}$$

where $\nu_i = (\nu_1, \nu_2, \eta_1, \eta_2)$ and the elements in the coefficient matrix $a_{ij}$ are given by

$$a_{11} = \nu_1 + \frac{Q - 2\nu_1 A_1 + \nu_2 A_3}{A}, \qquad a_{12} = \frac{\nu_1 A_3}{A},$$

$$a_{13} = -g_1' - \frac{\nu_1^2}{A}\frac{\partial A_1}{\partial \eta_1}, \qquad a_{14} = \frac{\nu_1 \nu_2}{A}\frac{\partial A_3}{\partial \eta_2}, \qquad a_{21} = -\frac{\nu_2 A_1}{A},$$

$$a_{22} = \nu_2 + \frac{Q - (\nu_1 + 2\nu_2)A_1 - 2\nu_2 A_2}{A},$$

$$a_{23} = -\frac{(\nu_1 + \nu_2)\nu_2}{A}\frac{\partial A_1}{\partial \eta_1} - \frac{\nu_2^2}{A}\frac{\partial A_2}{\partial \eta_1}, \qquad a_{24} = -g_2' - \frac{\nu_2^2}{A}\frac{\partial A_2}{\partial \eta_2},$$

$$a_{31} = \frac{A_1(A_2 + A_3)}{A}\left(\frac{\partial A_1}{\partial \eta_1}\right)^{-1}, \qquad a_{32} = \frac{A_1 A_3}{A}\left(\frac{\partial A_1}{\partial \eta_1}\right)^{-1},$$

$$a_{33} = \frac{Q + (\nu_1 + \nu_2)A_3 + \nu_1(A_2 - A_1)}{A},$$

$$a_{34} = \frac{A_1(\nu_1 + \nu_2)\partial A_3/\partial \eta_2 + \nu_1 A_1 \partial A_2/\partial \eta_2}{A\partial A_1/\partial \eta_1},$$

$$a_{41} = -\frac{A_1 A_3}{A}\left(\frac{\partial A_3}{\partial \eta_2}\right)^{-1}, \qquad a_{41} = -\frac{A_3(A_1 + A_2)}{A}\left(\frac{\partial A_3}{\partial \eta_2}\right)^{-1},$$

$$a_{43} = -\frac{A_3(\nu_1 + \nu_2)\partial A_1/\partial \eta_1 + \nu_2 A_3 \partial A_2/\partial \eta_1}{A\partial A_3/\partial \eta_2},$$

$$a_{44} = \frac{Q - (\nu_1 + \nu_2)A_1 + \nu_2(A_3 - A_2)}{A}. \tag{2.8}$$

Note that the dependence on the bottom topography enters through $\partial A_1/\partial \eta_1$ and the other derivatives of the layer areas, all of which must be prespecified. Specific examples will follow in the discussion of the BAM sill and narrows geometry.

The long-wave speeds are the eigenvalues of the matrix $a_{ij}$. In general, two pairs of eigenvalues and associated eigenvectors will arise, corresponding to first and second internal modes. When the background flow contains no shear, the first baroclinic modes will be characterized by displacements of the two interfaces that are in phase, as shown by the dashed curves in the center of Fig. 3b. This pair corresponds to the modes that would arise in a two-layer system created by removing our middle layer. The second pair corresponds to the second internal mode that, under conditions of no shear, is characterized by 180° out of phase excursions of the two interfaces, as shown by the dotted lines at the right of Fig. 3b. When shear is present in the background flow, the phase lags of the two modes are still zero or 180° unless the phase speed is complex, a situation not encountered for BAM shears and stratification.

When the two propagation speeds for the first internal modes have opposite sign, signals carrying information with that particular vertical structure can propagate in either direction, toward the Red Sea or the Gulf of Aden. In this case we call the flow *subcritical* with respect to the first internal modes. When both speeds have the same sign, propagation in only one direction is indicated and we call the flow *supercritical* with respect to those modes. When one or both of the two speeds is zero the flow is *critical*. Similar terminology is used in connection with the second internal modes. Critical conditions at any section in a strait is an indication of hydraulic control. Supercritical conditions at *any* section of the strait is usually an indication of critical flow elsewhere and, therefore, of hydraulic control.

## 3. The Hanish sill

Figure 4 shows the topography across the Hanish sill section. Central to our study is data from the upward-looking ADCP moored near the bottom of the deep central channel and capable of ranging within about 13 m of the surface. The position of this instrument is denoted B2 in Fig. 1. Also present was a salinity–temperature mooring (not shown) instrumented with six moored CTD units (Sea Cats) at depth levels of 145 m, 117 m, 94 m, 66 m, 52 m, and 30 m, deployed within 100 m of the ADCP. A continuous plot of along-axis, ADCP velocity profile over the period June 1995–March 1996 appears in Fig. 3 of Murray and Johns (1997). Also, Figs. 4a,b of that paper show temperature and salinity over the same period.

The dashed line in Fig. 4 is an approximation to the bottom topography used in the propagation speed cal-

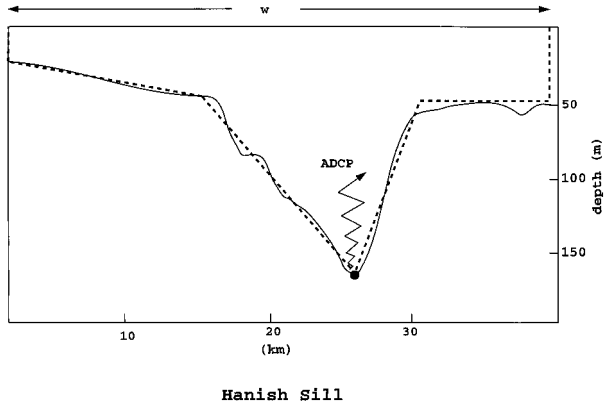


FIG. 4. Cross section of the central BAM at Hanish sill with instrumentation and analytical approximation (dashed curve) to bottom topography.

culation. The layer areas and their derivatives for this approximate topography are given by

$$A_1 = d_1 w - \frac{1}{2}\alpha(d_1 - 20)^2$$

$$A_2 = (45 - d_1)(w - 25\alpha) + \frac{1}{2}\alpha(45 - d_1)^2 + 65(118^2 - d_3^2)$$

$$A_3 = 65 d_3^2 \qquad \frac{\partial A_1}{\partial \eta_1} = -\frac{\partial A_2}{\partial \eta_1} = -w + \alpha(d_1 - 20)$$

$$\frac{\partial A_2}{\partial \eta_2} = -\frac{\partial A_3}{\partial \eta_2} = -130 d_3, \tag{3.1}$$

where $\alpha = 564$ and all other quantities are expressed in meters. These expressions are valid provided the upper interface depth is $<45$ m and the lower interface depth is $>45$ m, which is true in all months. The parameter $w$ is the width of the upper portion of the model channel (see Fig. 4) and is computed so as to remove the barotropic transport, as described below.

When configuring a layer model to match an observed flow with continuously varying velocity and density, there are always uncertainties in defining interface positions. There is often a range of reasonable choices, and we compute phase speeds over this range. We also vary the density values over a reasonable range when direct density information is not available (which is sometimes the case at the narrows). The ranges in phase speeds that result from all of these variations are not error bars in the strict sense, but they do give an indication of the uncertainty of the calculation due to ambiguities in fitting the layer model to the observed flow. We will refer to these ranges as ''uncertainty bar.''

The propagation speed calculations are based on monthly mean stratification and velocity. Figure 5 shows

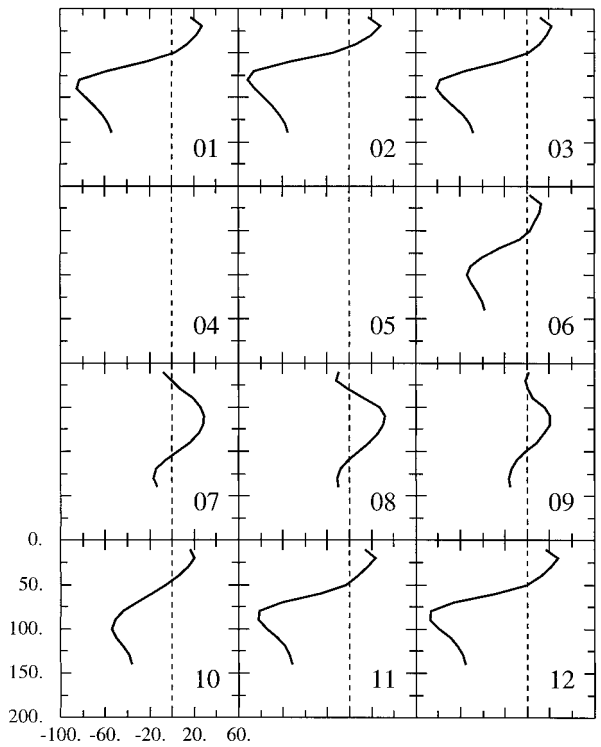


FIG. 5. Monthly mean ADCP velocities at Hanish sill, June 1995–March 1996. The bottom (not shown) is at 162 m.

the monthly mean ADCP sill velocity profiles.[2] Note the distinctive ''summer'' profiles of July through September, which contain Red Sea outflow (negative velocity) in the upper 10–20 ml, middepth inflow, and deep outflow. During these months the interfaces of our three-layer model are nominally chosen as the two zero crossings of the velocity profiles. For example, the August profile has nominal interface levels at $z \cong 25$ m and $z \cong 105$ m. The monthly mean velocity profile for August is then averaged over the three corresponding layers to obtain $u_1$, $u_2$, and $u_3$. The stratification measured at the salinity–temperature mooring is then used to compute monthly averaged densities and these are averaged over each of the three layers to form $\rho_1$, $\rho_2$, and $\rho_3$. We also vary the positions of the interfaces by $\pm 5$ m about the nominal values and include the results in our uncertainty bars.

The winter and transitional month (Oct–Jun) velocity profiles have inflow throughout the upper 40–50 m underlain by outflow so that the velocity has a two-layer character. However, the stratification throughout this time period has a three-layer structure, which can be

[2] For the purpose of calculating phase speeds, the profiles are extrapolated to the surface (from 20-m depth) and bottom (from 30 m above the bottom) using both constant velocity extensions and constant shear extensions. The results for each type of extrapolation are included in the uncertainty bars.

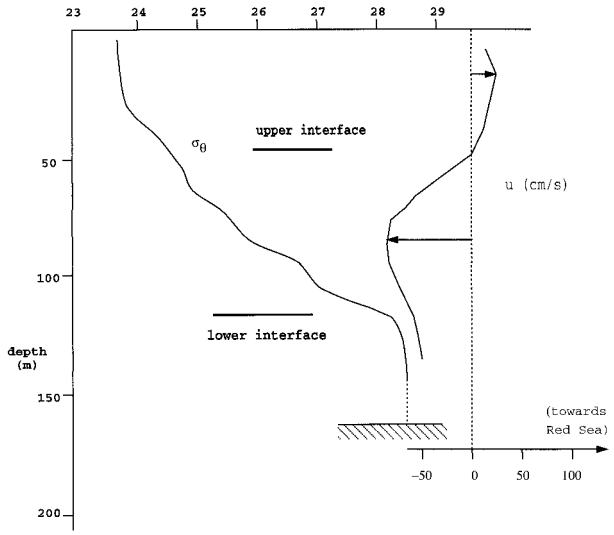


FIG. 6. April 1996 sill density profile shown with March 1996 ADCP velocity profile.

seen in the $\sigma_\theta$ profile made from an April 1996 CTD cast at the sill (Fig. 6.) A nearly homogeneous upper layer of thickness 30–40 m is underlain by a stratified middle layer of thickness ~80–90 m and a lower homogeneous layer of thickness ~40 m. Next to the $\sigma_\theta$ profile in Fig. 6 is the March 1996 ADCP velocity profile. The velocity zero crossing lies 15–20 m beneath the lower boundary of the upper homogeneous layer. The close proximity of these two boundaries is typical of the October–March data. In the intermediate layer the velocity reaches a maximum value (in the direction of the Gulf of Aden) and stratification is evident. In the lowest layer the density is relatively homogeneous and the velocity is reduced. For the picture shown in Fig. 6, we configure the three-layer model the following way: The lower interface is picked to match the top of the lower homogeneous layer (~120-m depth) and this level (which is less distinct than the lower interface position for summer) is varied by ±10 m. The upper interface is picked to match either the zero crossing of the velocity profile (~45-m depth) or the bottom of the homogeneous layer (~35-m depth). Wave speeds are calculated for both of the later choices, and the range in values is included in the uncertainty bar estimates. With this model configuration, the mode-1 wave speeds turn out to be close to what would be obtained from a two-layer model with the interface coincident with the velocity zero crossing. In fact, we perform a two-layer calculation[3] with the interface placed at the velocity zero crossing and include the results in the mode-1 uncertainty bars.

Note that most of the velocity profiles in Fig. 5 have a significant barotropic (depth averaged) component. For example, the depth-averaged velocity in November is more than $-25$ cm s$^{-1}$. On the other hand, it is known that the annual mean barotropic velocity in the BAM (based on a 2 m yr$^{-1}$ evaporation rate) is less than 1 cm s$^{-1}$ and monthly mean values are unlikely to exceed this by any significant amount. The apparent barotropic transports in the ADCP profiles are due to the fact that the upper layer is much wider than the lower layers. For example, the strongest negative velocities in November occur at about 85-m depth where the flow is confined to a narrow central trough, whereas the upper layer could extend over a much larger width (Fig. 4). For the purposes of phase speed calculation, it is desirable to remove the barotropic component of the flow. One could do so by simply adding a constant factor to the velocity profile, but, since the mass imbalance is almost certainly due to the relatively large (but unknown) width of the inflow, we *calculate* the width $w$ of the upper part of the model channel such that the total transport is zero: $u_1A_1 + u_2A_2 + u_3A_3 = 0$.[4]

Figure 7 shows the results of the propagation speed calculations for each month. (Note that the ''phase'' and ''group'' propagation speeds are identical for these long waves.) The left- and right-hand columns of arrows correspond to the first and second internal modes, respectively. Each arrow indicates the magnitude and direction of the speed of one of the two pairs of modes, with right-pointing arrows indicating propagation toward the Red Sea. Uncertainty bars appear near the tips of the arrows indicating the ranges in propagation speeds due to ambiguities in the definition of the interfaces, variations in reasonable values of the layer densities, and estimated errors in removing the barotropic transport. (The bars are omitted whenever their range is less than 5 cm s$^{-1}$). As an example, the two first internal modes corresponding to month 6 have speeds $\cong(-1.08$ to $-1.18$ m s$^{-1}$ and $+0.28$ to $+0.43$ m s$^{-1}$), indicating that the flow is subcritical with respect to the first internal modes. The $-1.08$ to $-1.18$ m s$^{-1}$ wave propagates toward the Gulf of Aden, while the other wave propagates toward the Red Sea. Similarly, the second internal modes for the same month have speeds $\cong(-0.65 \pm 0.03$ m s$^{-1}$ and $+0.06 \pm 0.03$ m s$^{-1}$), indicating nearly critical flow. That is, one wave prop-

[3] The two-layer phase speed is calculated by configuring the three-layer model to have a thin (1 m thick) intermediate layer with zero velocity and centered about the velocity zero crossing. This method gives mode-2 phase speeds that are very close to those of a two-layer model.

[4] In most cases, the resulting $w$ is within 30% of the actual strait width at 20-m depth, so the technique seems quite reasonable. In the few cases where this difference exceeds 30% we simply set $w$ to be the strait width (~100 km at the sill) and verify that the resulting barotropic velocity is small compared to the calculated propagation speed. Additionally, we vary $w$ within 20% of its estimated value in all cases to verify that the resulting phase speeds are insensitive to this value. The range in phase speeds resulting from this variation are included in the uncertainty bars.

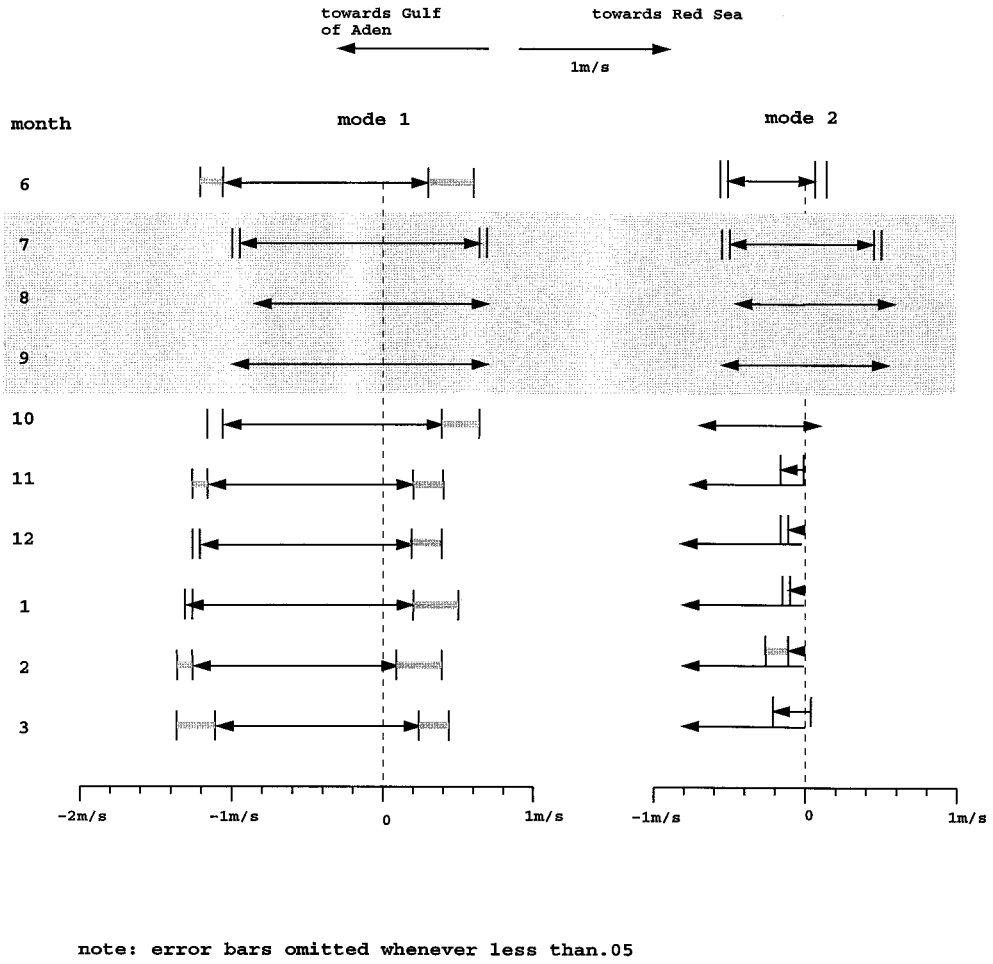


FIG. 7. Propagation speeds of the first and second long internal gravity wave modes at the Hanish sill. Each arrow indicates the magnitude and direction (toward or away from the Red Sea) of a particular wave based on mean velocity for that month. The net barotropic flow has been removed before calculation of the speeds. Uncertainty bars indicate ranges in calculated speed due to ambiguities in stratification and/or interface definition.

agates toward the Gulf of Aden, but the wave that would otherwise propagate toward the Red Sea is nearly arrested. The mode-2 propagation speeds were remarkably insensitive to variations in the definition of the interfaces and layer densities, as evidenced by the relatively small error bars.

Figure 7 shows that the flow is substantially subcritical with respect to both mode 1 and mode 2 during the summer (months 7–9). ''Substantially subcritical'' means that the two speed arrows for each mode point in opposite directions, that the two speeds have roughly the same magnitude, and that the magnitude is roughly the same as if the fluid was quiescent. During months 6 and 10–3 the flow continues to be subcritical with respect to mode 1, although the speeds of the wave attempting to propagate into the Red Sea are reduced. At one end of the uncertainty bars the flow is, in fact, close to being critical. The reduction in speed is particularly apparent in the winter months (11–2). It is possible therefore, that the sill is close to a point of mode-1 critical control.

With respect to mode 2 the flow is supercritical during months 2–3 and very close to the critical speed over months 6, 10–2, and perhaps 3. This behavior suggests the presence of a mode-2 critical control section at or near the sill during these months. Such a control would arrest the mode-2 wave attempting to propagate from the Gulf of Aden into the Red Sea. For this wave, the ratio of interfacial displacements $\eta_1/\eta_2$ is typically $-0.50$ in the winter months, meaning that a negative displacement of the lower interface is associated with a positive displacement of the upper interface of about half the magnitude.

## 4. The Perim narrows

Figure 8 shows the cross section of the strait at Perim narrows along with the position of the ADCP and an

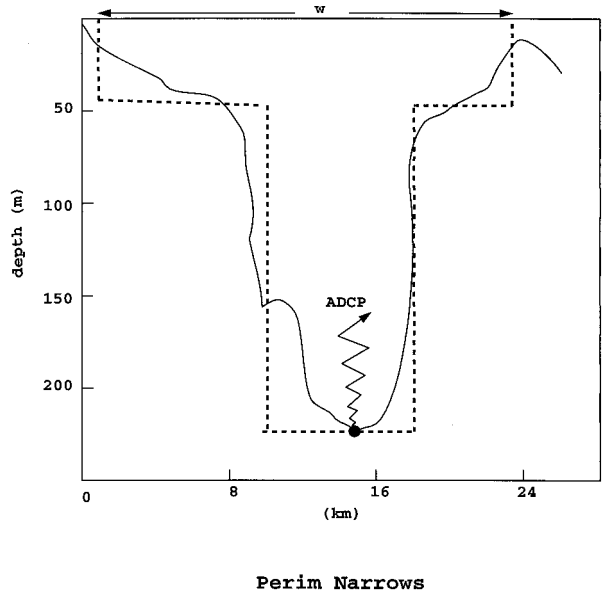


FIG. 8. Cross section of BAM at Perim narrows with instrumentation and analytical approximation to bottom topography.

analytical approximation of the topography. Here, the ADCP is capable of ranging to within 16 m of the surface. As in the case of the sill, the topography contains a deep central trough the depth of which ~220 m is greater than that ~163 m at the sill. The areas and their derivatives for the analytical topography are given by

$$A_1 = d_1 w, \qquad A_2 = w(55 - d_1) + 7200(165 - d_3),$$

$$A_3 = 7200 d_3, \qquad \frac{\partial A_1}{\partial \eta_1} = -\frac{\partial A_2}{\partial \eta_1} = -w,$$

$$\frac{\partial A_2}{\partial \eta_2} = -\frac{\partial A_3}{\partial \eta_2} = -7200. \tag{4.1}$$

These expressions are valid as long as the upper interface is shallower than, and the lower interface deeper than, 55 m. In some cases both interfaces lie below 55 m and (4.1) is replaced by

$$A_1 = 55w + 7200(d_1 - 55), \qquad A_2 = 7200 d_2,$$

$$A_3 = 7200 d_3, \qquad \frac{\partial A_1}{\partial \eta_1} = -\frac{\partial A_2}{\partial \eta_1} = \frac{\partial A_2}{\partial \eta_2} = -\frac{\partial A_3}{\partial \eta_2} = -7200. \tag{4.2}$$

As before, $w$ is computed so as to bring the total volume transport to zero and all quantities are expressed in meters. In all cases, the computed value of $w$ was within 30% of the actual width.

Monthly mean velocities are shown in Fig. 9 over June 1995–March 1996. Note the Red Sea outflow in the upper 10–15 m during July, August, and September. Also note that the velocity extremes are generally larger than at the sill. Unfortunately, there is a lack of complete

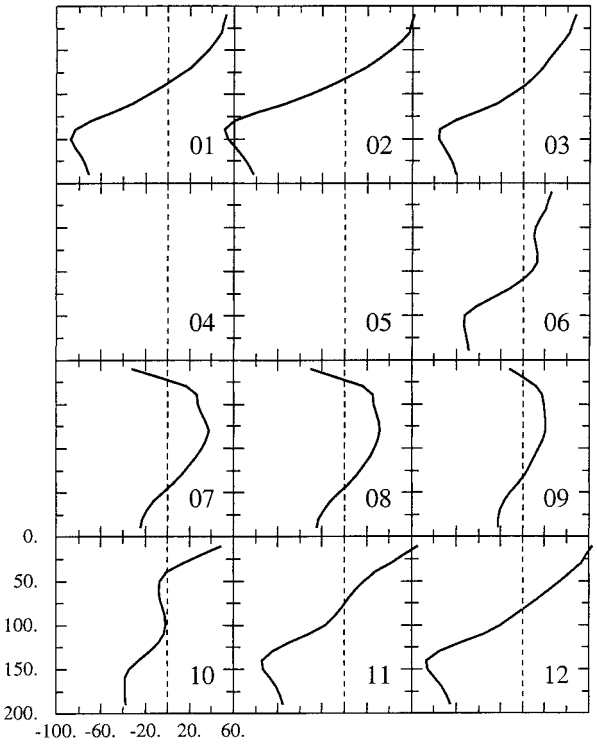


FIG. 9. Monthly mean ADCP velocities at Perim narrows, June 1995–May 1996. The bottom (not shown) is at 220 m.

density information at the narrows as the current here apparently caused intense strumming in the nearby *T–S* chain mooring with resultant instrument damage. Consequently, layer densities had to be calculated from a 1 June 1995 CTD cast in the central narrows and, during other months, inferred from the sill density. Some calculations were repeated using layer densities taken from hydrography appearing in Siedler (1968), Patzert (1974), Maillard and Soliman (1986), and Smeed (1997). The $\sigma_\theta$ profile from the June CTD cast is shown in Fig. 10 along with the June mean velocity profile. The three-layer structure in density is present, with an intermediate layer 130 m thick sandwiched between upper and lower homogeneous layers. Unlike the situation at the sill, the base of the upper homogeneous layer (~40 m) is no longer close to the zero crossing of the velocity (~120 m); however this is a peculiarity of the June flow, which is transitional between summer and winter. Probably more characteristic of winter are the 19 December velocity[5] and density profiles measured by Siedler (1968) in the central channel slightly south of the location of the Murray and Johns ADCP. (The position of Sielder's measurements are indicated by the small circle with the nearby S in Fig. 1.) Figure 11

[5] Direct current measurements were made by Siedler (1968) using a lowered Savonius current rotor.

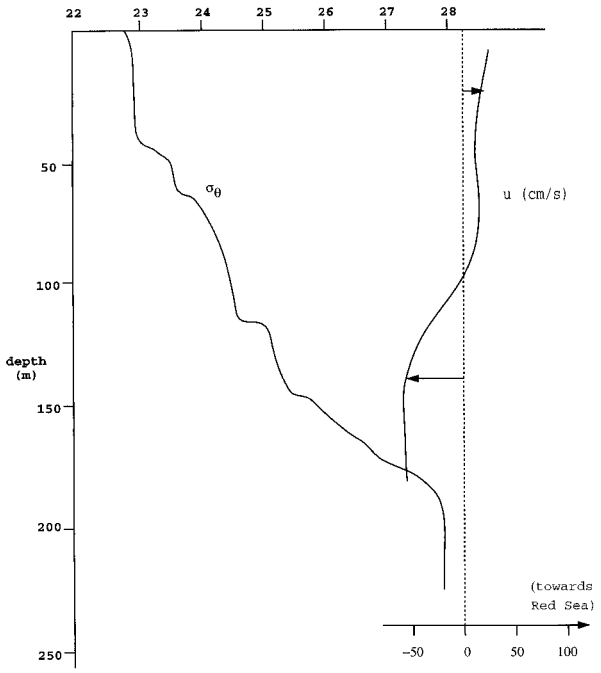


FIG. 10. June ADCP velocity profile at the Perim narrows, shown with a density profile taken from a near by June CTD cast.

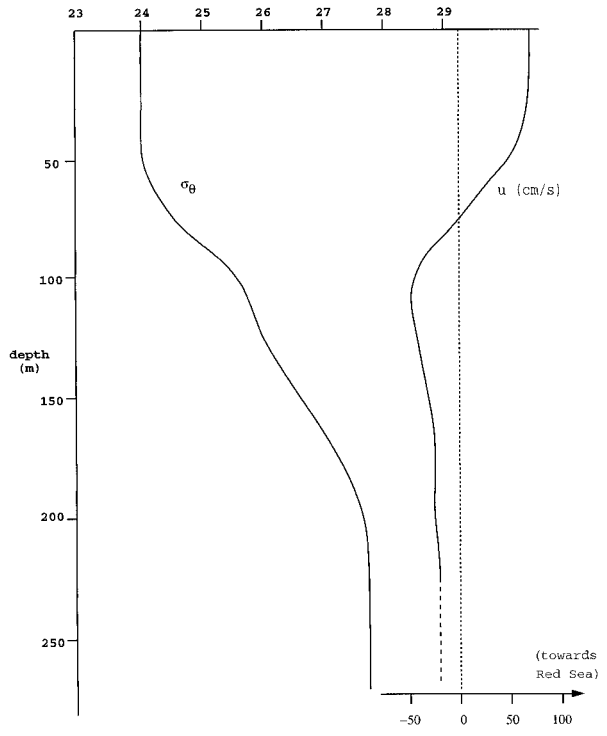


FIG. 11. December velocity and density profiles measured by Siedler (1968) at a cite approximately 8 km downslope (south) of our Perim narrows section. The location is shown in Fig. 1.

(constructed from Siedler's Figs. 43 and 44) contains the current speed and density profiles averaged over a three-day period. The base of the homogeneous layer lies at 50–60 m depth, while the velocity zero crossing lies at a depth ~70 m. Calculation of the phase speeds during the winter months was made following the same procedure as used at the sill.

The narrows phase speeds for each mode and each month are indicated in Fig. 12. In contrast to the situation at the sill, the narrows flow is substantially subcritical with respect to mode 1 for each month. The flow is also subcritical with respect to mode 2, though not substantially so throughout winter. In fact, the phase speed of the mode-2 wave attempting to propagate into the Red Sea is nearly zero over months 1 and 2 and relatively small during months 6, 11, 12, and 3. The value of $\eta_1/\eta_2$ for this wave in month 2 is $-0.25$, meaning that a negative displacement of the lower interface is associated with a displacement of the upper interface, which is positive but only ¼ as large.

The dashed representation of month 12 in Fig. 12 (designated ''Siedler'') shows a supplemental calculation based on direct current measurements made by Siedler (Fig. 11). The main difference between our month 12 findings and Siedler's is that his flow is substantially subcritical with respect to mode 2, whereas ours is marginally subcritical. This difference is due mainly to the greater bottom depth (270 m as opposed to <220 m) at his narrows section.

## 5. Hydraulic interpretation of the winter results

The strongest indications of critical control occur with respect to mode 2 at the sill during months 10–3 and 6. In order to understand the significance of this control it is necessary to further examine the composition of the two layers that compose the outflow in winter. The first consists of $\sigma_\theta$ ranging from 23 to 27.5, which according to the historical hydrography appearing in Patzert (1974), originates from the Red Sea thermocline (depths of approximately 50 to 125 m). The second consists of the relatively homogeneous bottom layer with $27.75 < \sigma_\theta < 28.2$, which originates from greater depths. That the lowest layer is so homogeneous is consistent with the fact that water deeper than about 125 m in the Red Sea is quite homogeneous, although mixing could also play a role.

To investigate the possibility of mixing within the outflow more carefully we have examined two June 1995 CTD casts, one at the sill (number 45, to 138-m depth) and one 11 km north of the sill (number 50, to 158-m depth). The *T*–*S* diagrams for both casts are shown in Fig. 13 over the depth ranges 98–138 m for number 45 and 110–158 m for number 50. The deepest waters ($T < 21.75$°C) are essentially identical, while higher up in the water column the salinity differences ($\Delta S \simeq 0.01$ psu) are close to exceeding the resolution of the instrument. The results suggest that little mixing

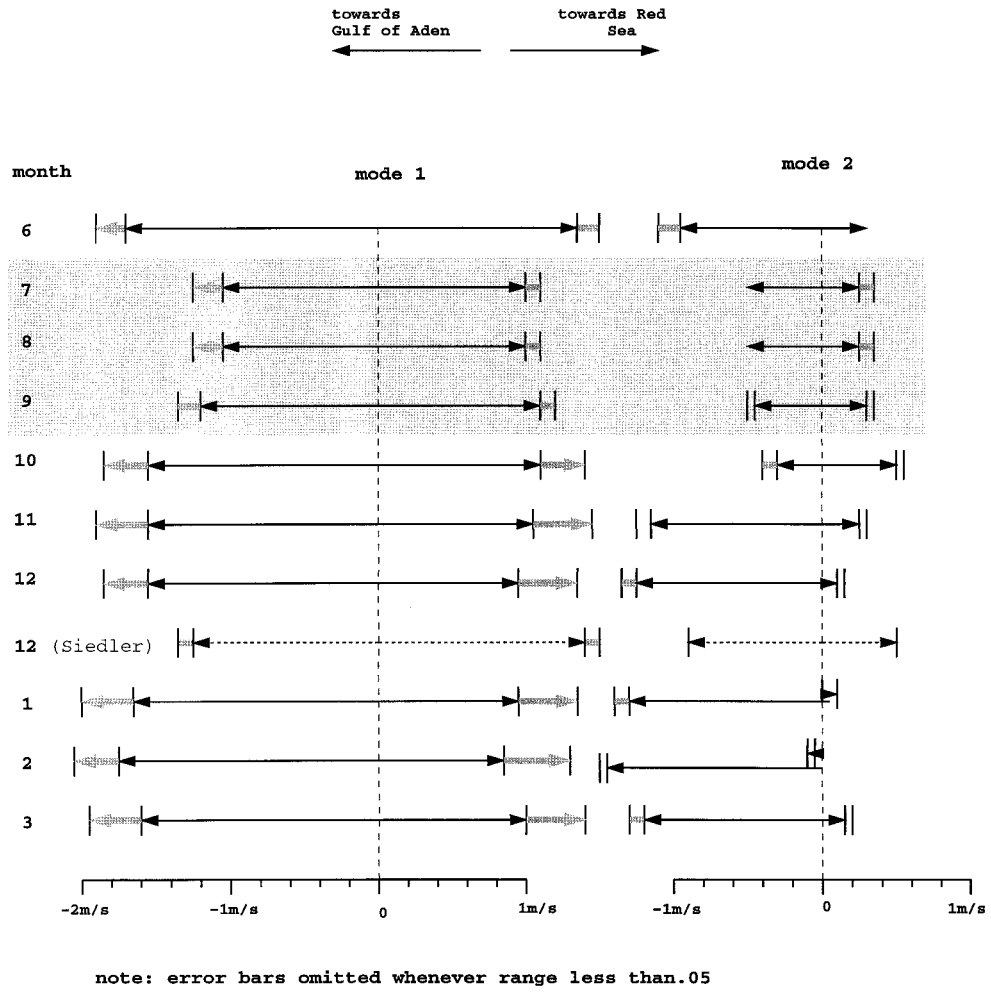


FIG. 12. Propagation speeds of the first and second long internal gravity waves modes at the Perim narrows. The representations are the same as in Fig. 7.

is taking place between the two locations and over the depths shown. Also, the bulk Richardson number

$$\frac{gD\Delta\rho}{\rho(\Delta U)^2}$$

of the outflow, calculated using a very liberal $\Delta U \leq 1.2$ m s$^{-1}$ over $D = 60$ m, is $>1.6$ m s$^{-1}$. This value also argues against mixing within the outflowing layer just upstream of the sill.

In an attempt to determine the extent to which the lower fluid is drawn up from greater depths, we have computed the average salinity over the lowest 40 m of CTD cast 45 and searched 40-m intervals of cast 50 to find the offset depth at which the average is the same. The two average salinities match ($\Delta S = 0$) at an offset of 25 m. That is, the deepest waters measured by the CTD cast on the sill comes from an average of 25 m deeper 11 km upstream. This ''aspiration'' of deeper water is entirely consistent with the Bryden and Stommel (1982) model, more recently emphasized by Kinder and Parrilla (1987) for the Gibraltar overflow.

The two outflowing layers are shown schematically in Fig. 14 and labeled Red Sea thermocline water (RSTW) and Upper Red Sea Deep Water (URSDW). Note that these layers have different sources; Red Sea Deep Water is formed sporadically during winter deep convection events in the far northern reaches of the Red Sea (Woelk and Quadfasel 1996), whereas the thermocline is thought to be replenished more continuously over a substantially larger area (Cember 1988; Eshel et al. 1994; Garrett et al. 1995; Eshel and Naik 1997). The near criticality of the sill (and perhaps narrows) flow with respect to mode 2 implies a certain degree of influence over the partitioning of volume transport between these two water masses.

The influence alluded to above can be illustrated by considering an example. We choose a February sill realization in which the mode-2 waves have propagation speeds $-0.81$ m s$^{-1}$ and $-0.04$ m s$^{-1}$. The flow is

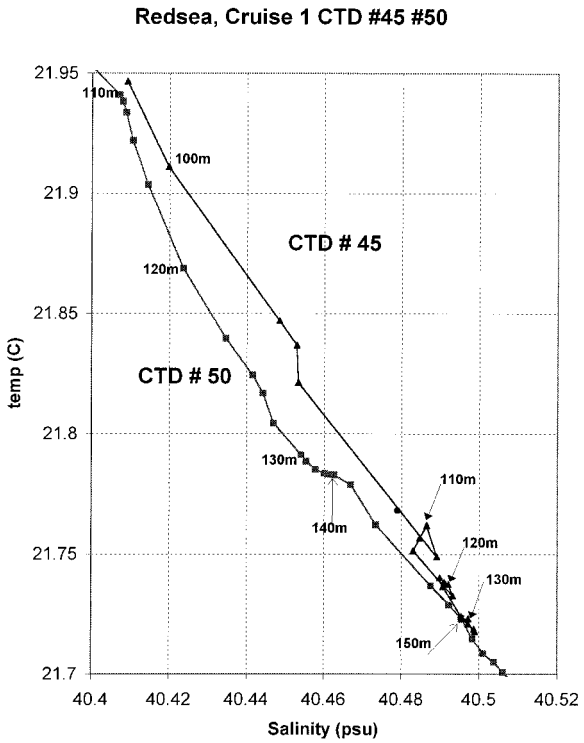


FIG. 13. Temperature–salinity plots for 3 June 1995 CTD casts 45 (taken at 1842 UTC 3 June 1995, at the Hanish sill) and 50 (taken at 0010, 4 June 1995, 11 km north of the sill). For cast 45, the data runs from 98 to 138 m, also in 2-m increments. For cast 50, the data is for depths 110–158 m at 2-m intervals.

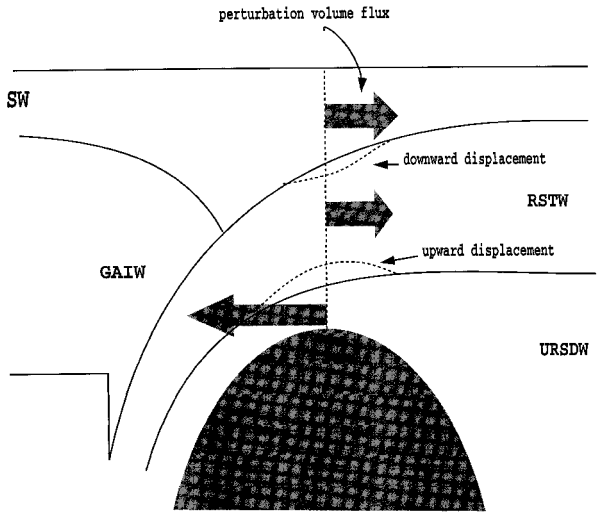


FIG. 14. A schematic representation of the structure of one of the mode-2 waves whose speed was calculated using the January sill values: $u_1 = 0.25$, $u_2 = -0.61$, $u_3 = -0.56$ m s$^{-1}$; $d_1 = 45$, $d_2 = 75$, $d_3 = 43$ m; and, $\rho_1 = 1.0237$, $\rho_2 = 1.026$, $\rho_3 = 1.0284$, which leads to $c = 0.04$ m s$^{-1}$ for this wave. The dashed lines indicate displacements of the interfaces, and the solid arrows perturbations of the two volume fluxes.

therefore very close to being critical with respect to the second internal mode. The wave whose speed is nearly zero has a vertical structure that causes perturbations of the layer volume fluxes in the proportions (1.00, 0.88, $-1.88$). That is, a volume flux perturbation of one unit in the upper layer is accompanied by a 0.88 change of the same sign in the middle layer and a 1.88 change of reverse sign in the lower layer. This situation is depicted in Fig. 14, which shows the flow rate perturbations as thick arrows in each layer. Changes in flow rate due to the presence of the wave are roughly equal in the middle and upper layer, and opposite and of twice the magnitude in the lower layer. Accompanying these perturbations are displacements of the two interfaces. For this wave (which has $\eta_1/\eta_2 = -0.50$) the perturbation flux arrows shown are associated with an upward displacement of the lower interface and a downward displacement, half as large, of the upper interface displacement. These displacements are shown by the dashed lines in Fig. 14. (Of course, there is no fixed sign for this linear disturbance, and we could also have drawn Fig. 14 with the flux arrows and displacements reversed.) The above picture is similar for all of the nearly critical, mode-2 disturbances of the steady flow at the sill during winter. The vertical structures of the disturbances suggest influence over the partitioning between the lowest layer transport and the transports in the upper two layers. That is, critical control with respect to the second internal mode is associated with regulation of the amount of Upper Red Sea Deep Water that is able to pass over the sill. Further analysis of this phenomena would require a more complete model.

## 6. Time dependence and rotation

Murray and Johns (1997) report typical barotropic tidal velocities of about 60 cm s$^{-1}$ and maximum tidal velocities of about 1 m s$^{-1}$ in the BAM. In addition, they measure mesoscale fluctuations with periods of 5–10 days, typical velocities of magnitude 20–50 cm s$^{-1}$, and with more complex vertical structure. Reference to the sill propagation speeds (Fig. 7) shows that the 60 cm s$^{-1}$ typical tide, and perhaps the 20–50 cm s$^{-1}$ mesoscale fluctuations, are sufficient in months 10–3 and 6 to reverse the sign the mode-1 wave that propagates toward the Red Sea, thereby creating mode-1 supercritical flow. During months 7–9, a 60 m s$^{-1}$ tide would not quite reverse the direction of these waves, though the maximum l m s$^{-1}$ tides would. At the narrows (Fig. 12) it appears that a 60 m s$^{-1}$ tide is insufficient to cause mode-1 supercritical flow in any month, though a 1 m s$^{-1}$ tide might occasionally be large enough. It is therefore quite possible that hydraulic control with respect to mode 1 at the sill, if it occurs, is highly intermittent. For mode-2, the intermittency is even more pronounced. All of the fluctuations mentioned above seem sufficient to change the direction of the disturbance that, in the absence of currents, would propagate into the Red Sea. Moreover, the tidal velocities might also reverse the sign

of the other mode-2 wave, particularly during the summer.

Our uncertainty bars do not reflect ambiguities resulting from tidal or mesoscale time variations or any uncertainty that might result from applying concepts developed in connection with steady flows to time-dependent flows. In general, the application of hydraulic theory to rapidly varying flows is a relatively unexplored issue. In some case studies involving more extensive measurements in space and time, it is possible to follow individual signals as they propagate though the strait in question. [An example is the undular bore observed in the Strait of Gibraltar (Armi and Farmer 1988; Farmer and Armi 1988).] A discussion of the hydraulics of instantaneous flows in the Bab al Mandab would require more extensive measurements and, probably, further advances in theory.

The importance of (neglected) rotation is typically estimated by calculating the width of the strait to the internal Rossby radius of deformation $L_d$. In the present model there is a distinct Rossby radius associated with each internal mode, and their values are estimated in the appendix to be 16 km $< L_d <$ 18 km for mode 1 and 10 km $< L_d <$ 12 km for mode 2. The appropriate width to compare these values of $L_d$ against is not obvious. The actual channel widths at the sill and narrows are wider than any of the $L_d$ estimated above. However, much of the actual width is covered by water that is homogeneous in our three-layer theory. This is particularly true in the winter and transitional months, when the upper interface lies near the top of the central topographic troughs and the lower interface lies beneath. Thus, the average width of these central troughs (about 7 km in both cases) is perhaps the appropriate scale to use. Based on these values we calculate (again in the appendix) that the error in estimating the appropriate long wave speed is less than 5%. The small error expectation is due to the fact that the role of long gravity waves in nonrotating hydraulics is played by Kelvin waves in rotating hydraulic models. The formulas for their speeds in the presence of a background flow are nearly the same.

On the subject of rotation, we also note that the May and June 1995 CTD survey carried out by Murray and Johns (1997) indicated very little cross-strait slope in isotherms and isopycnals at the sill or narrows, a further indication of the weakness of rotation.

## 7. Conclusions

Through direct calculation of internal long-wave speeds, we have attempted to assess the criticality of the flow at the Hanish sill and Perim narrows, the two primary choke points of the Bab al Mandab. Our results based on monthly mean velocity and stratification are quite surprising; we find that the flow at both of the sections is subcritical with respect to the first baroclinic mode (the mode involved in two-layer hydraulic control). In particular, our analysis suggests the monthly mean flow to be substantially subcritical at the Perim narrows throughout the entire deployment period (June 1995 through April 1996). Only the strongest tides might temporarily render the flow there supercritical. The same can be said for the Hanish sill flow during the ''summer'' months 7–9. During months 10–3 and 6 the flow is marginally to moderately subcritical, as evidenced by the relatively slow speed of the first baroclinic wave attempting to propagate from the Gulf of Aden into the Red Sea. The nearly critical nature of the flow at one end of the uncertainty bars may indicate the *proximity* of our sill section to a section of critical flow (a point of hydraulic control) or may simply indicate that no mode-1 control exists. For example, it is possible that bottom friction has shifted the control to the south of the sill in the manner described by Pratt (1986). Given the uncertainties in our estimates due to factors such as the neglect of rotation, idealization of the bottom topography and (especially) extrapolation of density and velocity, either conclusion is possible. In any case, the strength of the tides and mesoscale fluctuations in the strait strongly suggest the intermittent occurrence of mode-1 critical flow.

Interpretation of results for the second baroclinic (mode 2) depends upon the season in question. During months 7–9, the monthly mean velocity has a three-layer character, with outflowing surface and Red Sea overflow waters and inflowing Gulf of Aden Intermediate Water. We configure our three-layer model such that the two interfaces correspond to the velocity zero crossings and calculate the mode-2 wave speeds accordingly. This calculation suggests the month 7–9 flow to be subcritical at both the sill and narrows, but perhaps subject to intermittent criticality or supercriticality at the hands of the strongest tides. During the remaining months, the velocity structure is two-layer in character but the density structure is more complicated. An upper, nearly homogeneous layer, which more or less corresponds to inflowing water, is underlain by an intermediate layer of stratified water originating largely from the Red Sea thermocline. Below this layer lies a nearly homogeneous layer of upper Red Sea Deep Water. When configured in accordance with this three-layer structure, our propagation speed calculations indicate nearly critical flow at both the sill and narrows. The wave whose speed is arrested is the one which, in the absence of any fluid velocity, would propagate from the Gulf of Aden into the Red Sea. The dynamics of this wave are such as to affect a partitioning between the volume flux of Upper Red Sea Deep Water and that of the two overlying layers. That is, the wave plays a role in determining how much Upper Red Sea Deep Water is drawn over the sill. Since the flow is close to critical at both the sill and narrows the actual point of hydraulic control is ambiguous. It might be the case that critical flow exists at both locations, with a hydraulic jump between. The situation is further complicated by the presence of

tides and mesoscale fluctuations that may render such a control intermittent.

*Acknowledgments.* This work was support by the Office of Naval Research under Grants N0014–95-1-0456 and N0014-95-1-0025. Eddie Weeks of LSU and Rainer Zantopp of RSMAS processed the ADCP and hyrographic data used to calculate phase speeds. We also wish to thank Heather Deese, David Fratantoni, Nelson Hogg, and David Smeed and two anonomous reviewers for a number of helpful comments.

## APPENDIX

### Estimates of the Importance of Rotation

The strength of (neglected) rotation can be approximated by comparing the Rossby radius of deformation for the vertical mode in question to some measure of the flow width. For a two layer flow, the Rossby radius of deformation is given [Pratt and Armi 1990, Eq. (2.8a)] as

$$L_d = [g(\rho_3 - \rho_1)D_{1\infty}D_{2\infty}/\rho_1(D_{1\infty} + D_{2\infty})]^{1/2}/f, \quad \text{(A1)}$$

where $f$ is the Coriolis frequency and $D_{1\infty}$ and $D_{2\infty}$ are the ''potential depths'' of the two layers, here numbered 1 and 2. In idealized situations, the potential depth of a layer is its upstream thickness in quiescent regions of the gulf or sea from which it originates. For example, $D_{2\infty}$ would be the upstream thickness in the Red Sea of the overflow water, perhaps 100–500 m, while $D_{1\infty}$ is the upstream thickness in the Gulf of Aden of the inflowing surface water, perhaps 100 m. Using this range of potential thicknesses as well as $g' = 0.004\ g$, and $f = 10^{-4}\ \text{s}^{-1}$ gives 16 km $< L_d <$ 18 km. For mode 2, no expression comparable to (A1) has yet been developed; however, we expect that the appropriate value of $L_d$ can be obtained by reducing the values of the potential depths and $g'$ by two-thirds, in which case (A1) gives 10 km $< L_d <$ 12 km.

The appropriate width to compare these values of $L_d$ against is not obvious. The actual channel widths at the sill and narrows are wider than any of the $L_d$ estimated above. However, much of the actual width is covered by water that is homogeneous in our three-layer theory. This is particularly true in the winter and transitional months, when the upper interface lies near the top of the central topographic troughs and the lower interface lies beneath. Thus, the average width $w_a$ of these central troughs (about 7 km in both cases) is perhaps the appropriate scale to use.

The rotational effect that impacts this study the most is the alteration in the propagation speed of long waves. With rotation, the long internal gravity waves that we have discussed become channel Kelvin waves. It is well known (Gill 1977) that the latter play the same role in rotating hydraulics that long gravity waves play in nonrotating hydraulics. To estimate the degree to which rotation might alter the phase speed, suppose that the deep central channel is replaced by a rectangular channel of width 6 km that contains two layers, one of them inactive. Then the speed of the long gravity wave and its Kelvin wave counterpart differ by the factor

$$\alpha = 1 - [1 - \tanh^2(w_a/2L_d)(1 - \overline{d}/D_\infty)]^{1/2}$$

[see Pratt 1983, Eq. (3.19), for example]. Using the worst case scenario, we take $w = 6$ km, $L_d = 10$ km, and $\overline{d}/D_\infty = 0.2$, which gives $\alpha = 0.04$, or a 4% error in propagation speed. (The average of the side wall depths is $\overline{d}$). Although rotation may be marginally important in the central trough, the associated errors in propagation speeds are probably not so.

## REFERENCES

Armi, L., and D. M. Farmer, 1988: The flow of Atlantic water through the Strait of Gibraltar. *Progress in Oceanography*, Vol. 21, Pergamon, 1–105.

Baines, P. G., 1995: *Topographic Effects in Stratified Flows*. Cambridge University Press, 482 pp.

Bower, A. S., H. D. Hunt, and J. F. Price, 1999: The character and dynamics of the Red Sea and Persian Gulf outflows. *J. Geophys. Res.*, in press.

Bryden, H. L., and H. M. Stommel, 1982: Origin of the Mediterranean outflow. *J. Mar. Res.,* **40,** 55–71.

Cember, R. P., 1988: On the sources, formation, and circulation of Red Sea deep water. *J. Geophys. Res.*, **93** (C7), 8175–8191.

Eshel, G., and N. Naik, 1997: Climatological coastal jet collision, intermediate-water formation and the general circulaion of the Red Sea. *J. Phys. Oceanogr.,* **27,** 1233–1257.

——, M. A. Cane, and M. B. Blumenthal, 1994: Modes of subsurface, intermediate, and deep water renewal in the Red Sea. *J. Geophys. Res.,* **99** (C8), 15 941–15 952.

Farmer, D. M., and L. Armi, 1986: Maximal two-layer exchange over a sill and through the combination of a sill and contraction with barotropic flow. *J. Fluid Mech.,* **164,** 53–76.

——, and ——, 1988: The flow of Mediterranean Water through the Strait of Gibraltar. *Progress in Oceanography*, Vol. 21, Pergamon, 1–105.

Fedorov, K. N., and S. L. Mechanov, 1988: Structure and propagation of Red Sea waters in the Gulf of Aden. *Oceanology,* **28,** 279–284.

Garrett, C., K. Speer, and E. Tragou, 1995: The relationship between water mass formation and the surface buoyancy flux, with application to Phillips' Red Sea model. *J. Phys. Oceanogr.,* **25,** 1696–1705.

Gill, A. E., 1977: The hydraulics of rotating-channel flow. *J. Fluid Mech.,* **80,** 641–671.

Kinder, T., and G. Parrilla, 1987: Yes, some of the Mediterranean outflow does come from great depth. *J. Geophys. Res.,* **92** (C3), 2901–2906.

Maillard, C., and G. Soliman, 1986: Hydrography of the Red Sea and exchanges with the Indian Ocean in summer. *Oceanol. Acta.,* **9** (3), 249–269.

Maxworthy, T., 1997: A frictionally and hydraulically constrained model of the convectively driven mean flow in partially enclosed seas. *Deep-Sea Res.,* **44,** 1339–1354.

Murray, S. P., and W. Johns, 1997: Direct observations of seasonal exchange through the Bab el Mandab Strait. *Geophys. Res. Lett.,* **24,** 2557–2560.

Patzert, W. C., 1974: Wind induced reversal in the Red Sea circulation. *Deep-Sea Res.,* **21,** 109–121.

Phillips, O. M., 1966: On turbulent convection currents and the circulation in the Red Sea. *Deep-Sea Res.,* **13,** 1149–1160.

Pratt, L. J., 1983: On inertial flow over topography. Part I. Semi-geostrophic adjustment to an obstacle. *J. Fluid Mech.*, **131,** 195–218.

——, 1986: Hydraulic control of sill flow with bottom friction. *J. Phys. Oceanogr.*, **16,** 1970–1980.

——, and L. Armi, 1990: Two-layer rotating hydraulics: Strangulation, remote and virtual controls. *Pure Appl. Geophys.*, **133,** 588–617.

Siedler, G., 1968: Schichtungs- and bewegungsverhaltnisse am sudausgang des roten meeres. ''*Meteor*'' *Forschungsergeb.*, **A4,** 1–76.

Smeed, D., 1997: Seasonal variation of the flow in the strait of Bab al Mandab. *Oceanol. Acta*, **20,** 773–781.

Woelk, S., and D. Quadfasel, 1996: Renewal of deep water in the Red Sea during 1982–1987. *J. Geophys. Res.*, **101** (C8), 18 155–18 165.